Permafrost-related landslides following a 2017 wildfire, Dempster Highway, Yukon (parts of NTS 116G/9 and 116H/12)

Heather C. Clarke *
Simon Fraser University

Derek C. Cronmiller
Yukon Geological Survey

Brent C. Ward
Simon Fraser University

Katelyn A. Groeneveld
Simon Fraser University

Clarke, H.C., Cronmiller, D.C., Ward, B.C. and Groeneveld, K.A, 2024. Permafrost-related landslides following a 2017 wildfire, Dempster Highway, Yukon (parts of NTS 116G/9 and 116H/12). *In*: Yukon Exploration and Geology Technical Papers 2023, L.H. Weston and Purple Rock Inc. (eds.), Yukon Geological Survey, p. 17–36.

Abstract

The Yukon is experiencing impacts of climate change, marked by elevated annual air temperatures, alterations in precipitation patterns and increased wildfire activity. These changes can lead to permafrost degradation, impacting highways and community infrastructure. In July 2017, a wildfire burned a slope in permafrost terrain above the Dempster Highway in the Yukon. In the years following the wildfire, two types of permafrost-related landslides have been observed on the slope. Active layer detachment activity was highest in the first year after the landslide, possibly influenced by warm temperatures and rainfall events. Retrogressive thaw flow slides formed in 2019 in areas of ice-rich permafrost and are still active in 2023. Deposition of sediment and influx of water has resulted in flooding near the highway, further degrading the permafrost in the valley bottom. This study characterizes the landslide timing and morphology following a wildfire on permafrost terrain, and investigates potential triggers and controls.

Introduction

Background

Northern regions are experiencing impacts due to climate change at a faster and more extreme rate than the rest of the world (Vincent, 2020). Over the last 50 years, the Yukon has seen an increase in mean annual air temperature of approximately 2°C, with the greatest increase in temperature occurring in winter (Perrin and Jolkowski, 2022). Temperatures are predicted to continue to increase, as are the intensity, frequency and annual amount of precipitation (Perrin and Jolkowski, 2022).

One of the major impacts of climate change in the Yukon is the alteration of permafrost conditions. Permafrost, defined as ground that remains below 0°C continuously for two or more years, plays a critical role in regulating various geomorphological processes and supporting unique ecosystems (Smith *et al.*, 2022). Thaw of permafrost and associated ground ice can lead to surface subsidence and slope instability, which modifies terrain and drainage patterns (Lewkowicz, 1990). Permafrost also plays a critical role in the global climate system: long-term climate warming can release carbon stored in near-surface permafrost as well as impact the

* heather_clarke@sfu.ca

amount and distribution of snow cover, which insulates and modifies the temperature of the underlying ground. The feedback loops triggered by thawing permafrost, such as the release of methane and carbon dioxide, further contribute to the amplification of global climate change (Jorgenson *et al.*, 2010; Schuur *et al.*, 2015). The geotechnical and environmental problems associated with permafrost degradation are increasingly important issues in the Yukon (Perrin and Jolkowski, 2022).

Permafrost distribution is primarily controlled by mean annual air temperature; other important factors include depth and duration of snow cover, slope angle, slope aspect, geology, surface water conditions and vegetation cover. Because of this, permafrost stability is threatened not only by the increasing mean annual air temperature, but also by factors including the alteration of precipitation patterns and increased frequency and severity of wildfires in the north (Smith *et al.*, 2022). Although wildfire activity varies annually, there is a regional trend in historical data from 1959 to 2015 of increased area burned per year and an increased number of large fires per year (Hanes *et al.*, 2019; Perrin and Jolkowski, 2022). The number and intensity of fires is expected to increase in Canada due to climate change (Wotton *et al.*, 2017); this will have significant impacts on permafrost conditions. Following fires, ground temperatures and active layer thicknesses increase, especially in more severely burned areas (Lipovsky *et al.*, 2005; Coates, 2008; Holloway *et al.*, 2020; Smith *et al.*, 2022). Wildfires destroy the insulating organic layer, reduce snow interception by trees due to the decrease in vegetation canopy, lower ground surface albedo by charring the organic mat, and diminish evapotranspiration (Lipovsky *et al.*, 2005; Smith *et al.*, 2022). The duration and extent of permafrost degradation after a fire can persist for years, depending on the burn intensity and the pre-fire vegetation cover (Holloway *et al.*, 2020). Measurements taken at burned and unburned sites in permafrost regions have shown the mean annual ground surface temperatures at burned sites were 1–7°C higher than at unburned sites (Holloway *et al.*, 2020).

In 2017, a wildfire initiated by a lightning strike burned 86 128 ha near the Dempster Highway in the Yukon during the span of three weeks from late June to mid-July (Yukon Wildland Fire Report, 2017). In the weeks and years following the fire, landslide activity was observed on a slope parallel to the highway, with one slide crossing the highway and forcing closure of the road until debris could be cleared. The purpose of this study is to characterize the timing and morphology of the landslides and explore potential relationships between permafrost characteristics, geology, weather conditions and ground disturbance. This work will contribute to the growing body of research on how climate change is impacting communities and infrastructure in permafrost regions.

Study area

Location and physiography

The study area encompasses the slopes parallel to KM 240 to KM 250 on the northwest side of the Dempster Highway, Yukon (Fig. 1), a 740 km all-season gravel highway beginning approximately 40 km south of Dawson City, Yukon, and traversing northeast across the Arctic Circle to the town of Inuvik, Northwest Territories. The study area overlaps with the Traditional Territories of the Tr'ondëk Hwëch'in and Vuntut Gwitchin First Nations. The highway here is part of the Ogilvie maintenance section and is bounded by the Ogilvie River on the southeast and a slope on the northwest. The Ogilvie River drains to the northeast, becoming the Peel River at its confluence with the Blackstone River 40 km northeast of the study area. The elevation ranges from 480 m above sea level (masl) near the Ogilvie River, up to 850 masl at the top of the slope.

The Eagle Lowland physiographic region is part of the Foreland fold and thrust belt, composed of deformed sedimentary rocks deposited on or adjacent to the stable North American craton (Smith *et al.*, 2004). Bedrock comprises uplifted sedimentary rocks from the Monster assemblage that were deposited during the Cretaceous (Dixon, 1992). These rocks include coarsening-upward cycles up to 30 m thick of dark grey to black shale with interbeds of siltstone and fine-grained sandstone (Dixon, 1992). The topography of the Eagle Lowland slopes is strongly influenced by bedrock structure and lithology, which influences slope angles and forms benches and terraces through differential erosion of rock types.

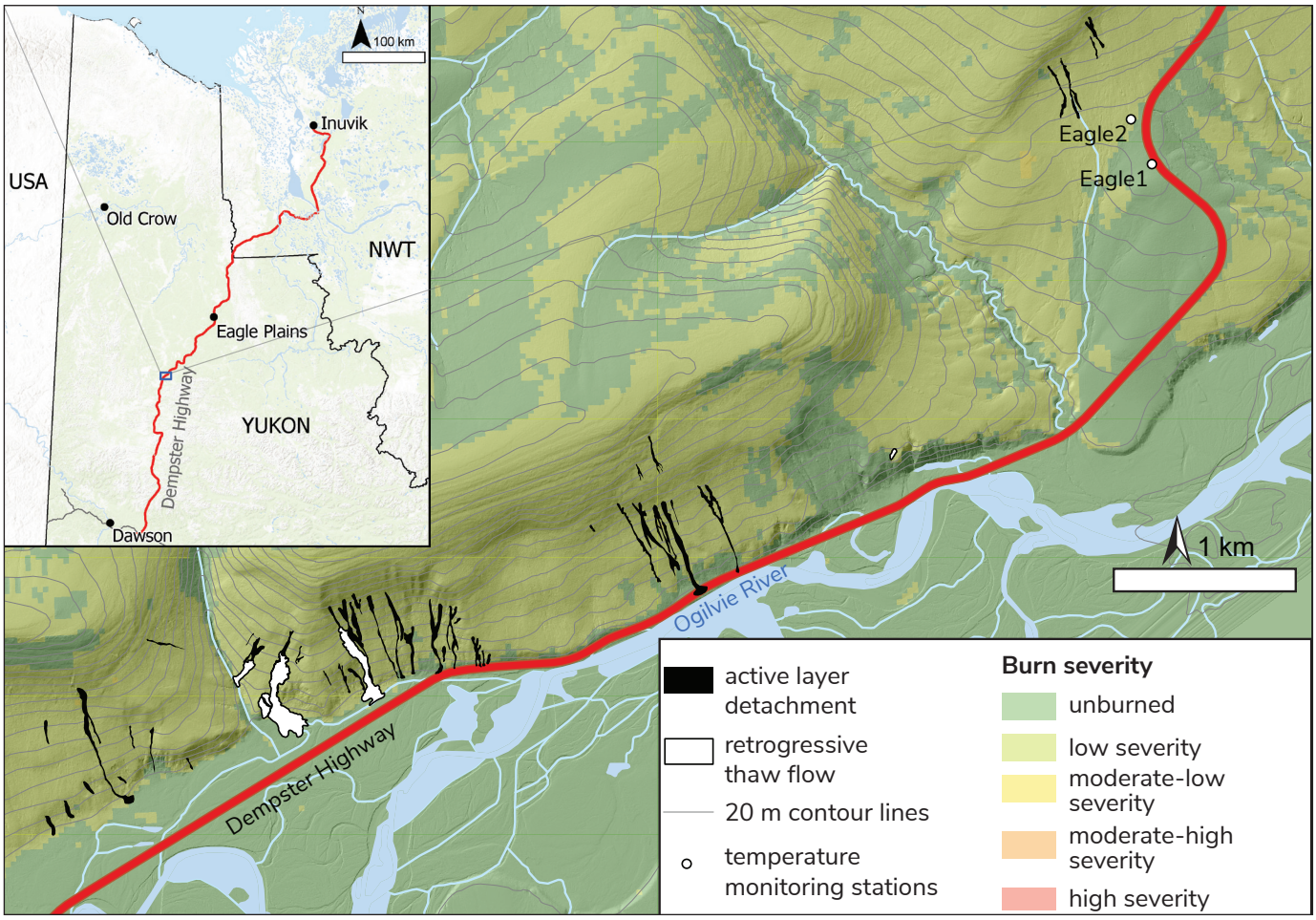

Figure 1. *Study area location with outlines of permafrost-related landslides from 2017 to 2023. Colour scale represents burn severity from the 2017 wildfire. Inset map shows regional location of study area. Dempster Highway represented by red line in both maps. The Ogilvie floodplain temperature monitoring site is not shown.*

Glacial history and surficial geology

The study area remained unaffected by glacial ice during the Quaternary; however, major rivers in the watershed were influenced by regional glaciation to the east. During this period, advancement of the Laurentide Ice Sheet northwest across the northern Mackenzie Mountains impounded the east-flowing Bonnet Plume basin and resulted in the formation of Glacial Lake Hughes during the Last Glacial Maximum (Duk-Rodkin and Hughes, 1995; Kennedy et *al.*, 2010). The glacial lake extended westward from the Bonnet Plume basin to the Ogilvie River valley and drained north via the Eagle River into the Bell basin (Duk-Rodkin and Hughes, 1995). The study area lies just beyond the mapped limits for Glacial Lake Hughes.

Continental glaciation also modified global circulation patterns and caused sea level to lower during glacial periods. During the Last Glacial Maximum, the exposed continental shelf between eastern Russia and Alaska, USA, formed the Bering Land Bridge, connecting the two continents. This unglaciated region is known as Beringia and was characterized by a cold and arid climate comprising tundra, steppe tundra and forest-tundra ecosystems (Guthrie, 2001). In the study area, the Ogilvie River system has incised the terrain, forming valleys and floodplains composed of fluvial materials. On the slope above the highway, aeolian accumulations of silt have formed thick packages of loess on slope breaks. Extensive weathering of the bedrock has resulted in the accumulation of colluvial blankets and veneers covering the slope.

Climate and vegetation

The study area is in the Taiga Cordillera Ecoregion, which is characterized by a subarctic continental climate with long, cold winters and short, cool summers (Smith *et al.*, 2004). Strong temperature inversions occur in this mountainous region due to topographic shading and cold-air drainage, causing the valleys to be considerably colder in the winter than the surrounding ridges and plateaus (Burn, 1994). Weather systems coming from the Gulf of Alaska lose most of their moisture on the St. Elias Mountains before reaching central Yukon; however, moderate precipitation occurs primarily as summer rainfall from June to August (Burn *et al.*, 2015). Annual precipitation is predicted to increase by 11% between 2021 and 2050 based on the representative concentration pathway (RCP) 8.5 emissions scenario, where greenhouse gas emissions continue to increase at current rates (Climate Atlas of Canada, 2019). Under the same scenario, summer and winter precipitation is expected to increase by 10 and 11%, respectively, with more heavy precipitation days (more than 10 mm in 24 hours) annually (Climate Atlas of Canada, 2019).

The closest weather station to the study site is located at the Ogilvie Highway maintenance camp at KM 194 of the Dempster Highway (Environment Canada, 2023). There are large gaps in the record from this station during the past two decades; however, from 1988 to 2006, the mean annual air temperature at the station was –9°C. The coldest month was January, with average monthly temperatures as low as –40°C, and the warmest month was July, with average monthly temperatures as high as 15°C (Environment Canada, 2023). Data from the weather station reveal an upward trend in the mean annual air temperature consistent with regional model predictions of a 1.3°C and 3.2°C increase in mean summer and winter temperatures, respectively, from 2021 to 2050 under the RCP 8.5 emissions scenario (Climate Atlas of Canada, 2019).

Vegetation in the study area features an open canopy forest of single and mixed-species canopies including black spruce (*Picea mariana*), white spruce (*P. glauca*) and aspen (*Populus tremuloides*). Canopy gaps are commonly filled with willow (*Salix* spp.) and alder (*Alnus* spp.), as well as shrubs and sedges such as dwarf birch (*Betula* spp.) and Labrador tea (*Rhododendron groenlandicum*). Willow, alder, balsam poplar (*P. balsamifera*) and aspen are present in the fluvial plain. Low-shrub tundra communities including dwarf birch, willows, and lichens are found on the upper slope and ridge.

Permafrost

Permafrost is continuous in the study area. Perennially frozen ground is present everywhere except locally under lakes, river channels and other bodies of water (Smith *et al.*, 2004). Ground ice content in permafrost regions influences the ground thermal regime and is an important factor in how the landscape will respond to permafrost degradation (French, 2017). Models have predicted that the study area has 10–20% ground ice content by volume in the upper 5 m of permafrost as either ice wedges or segregated ice (Heginbottom *et al.*, 1995; O'Neill *et al.*, 2022). These models are useful for regional and circumpolar estimations; however, the scale is not intended for site-specific conditions. More work is needed to better understand and predict ground-ice content at a local scale.

Landslide types

Two types of permafrost-related landslides occur in the study area: active layer detachments (ALDs) and retrogressive thaw flows (RTFs). Active layer detachments are rapid mass movements that occur when the active layer (the uppermost layer that freezes and thaws seasonally) becomes detached from the underlying permafrost (Lewkowicz, 1990; Lewkowicz and Harris, 2005a, b). The permafrost table serves as the failure plane for ALDs and controls the depth of scour. The initiation of ALDs involves a reduction of effective stress at the transition between the active layer and the permafrost table due to an increase in pore water pressure (Lewkowicz, 1990). Increased pore water pressure, which is commonly a result of precipitation or heat, can induce rapid thaw of ice-rich sediment at the transition layer (French, 2017). Other factors that influence the occurrence of ALDs include soil moisture conditions, slope form and steepness, surficial materials, depth of the active layer, and vegetation cover (Lipovsky *et al.*, 2005). Active layer detachments in the Yukon commonly involve flow or slide styles of movement and initiate on moderate to steep slopes. Wildfires can contribute to ALD initiation by rapidly thawing and deepening the active layer and melting ice at the transition layer, resulting in an increase in pore water pressure at the permafrost

table (Lewkowicz and Harris, 2005a; Coates, 2008). Destroying the vegetation reduces root strength in the organic mat and can lead to changes in permafrost conditions, impacting slope stability for months and years following a wildfire (Holloway *et al.*, 2020).

Retrogressive thaw flows are characterized by a steep, bowl-shaped headscarp of thawing ice-rich sediments or massive ice, and a low-angle tongue of landslide debris (Lantuit and Pollard, 2007). Initiation of RTFs commonly occurs when ground ice is exposed by processes such as fluvial erosion, subsidence, active layer detachments, wildfire, increased air temperatures, and human-induced ground disturbance (Kokelj *et al.*, 2015). As ice within permafrost melts, the structural integrity of the slope decreases and the headwall can retrogress upslope as further permafrost is exposed (Burn and Lewkowicz, 1990; Kokelj *et al.*, 2015). Retrogressive thaw flows deposit saturated material at the base of the headwall, which can be transported downslope by slides and flows at rates that are dependent on slope angle, sediment characteristics, and ground-ice content (Kokelj *et al.*, 2015). Retrogressive thaw flows farther north on the Dempster Highway had 20 year average retreat rates of 7.2–26.6 m/year (Lacelle *et al.*, 2015). The Takhini River retrogressive thaw slump (near Whitehorse) had a 6 year average rate of 8 m/year (Calmels *et al.*, 2021). Retrogressive thaw flows can undergo polycyclic cycles of stabilization and re-exposure for up to 50 years following the initial event (French, 1974). Both types of permafrost landslides can damage infrastructure and contribute large amounts of sediment and water into nearby terrestrial and aquatic ecosystems, altering ground temperatures and inducing change in vegetation growth (Jones *et al.*, 2021).

Methodology

Initial site investigations by the Yukon Geological Survey occurred in fall 2021 and fall 2022. In fall 2022, thermistors were installed in three locations (Table 1, Fig. 2): two in the study area, one in an unburned site (Eagle1) and the other in a burned site (Eagle2); and a third in an unburned site on the Ogilvie River floodplain (Ogilvie floodplain), approximately 4 km southeast of the study area. In 2023, fieldwork took place during three separate trips in June, August and September. Field observations were made at multiple landslides and samples were collected for geochronology, ice-content measurements and geotechnical analysis. The most active RTF during field investigations in 2023 was RTF1. To gain insight into the ice content of the headwall of RTF1, six sediment samples were taken from four stratigraphic units in the headwall. Volumetric excess ice content (E_i, expressed as a percentage) was estimated using equation 1 (Kokelj and Burn, 2003):

$$E_i = \frac{(W_V 1.09)}{(S_V + (W_V 1.09)} \quad (1)$$

where W_v is the volume of supernatant water, S_v is the volume of saturated sediment, and 1.09 represents the expansion of water when it freezes. Gravimetric ice

Table 1. *Site characteristics of temperature monitoring stations in the study area. The locations of Eagle1 and Eagle2 are shown in Figure 1; Ogilvie floodplain is approximately 4 km south of study area.*

Site	Eagle1	Eagle2	Ogilvie floodplain
Burn condition	unburned	burned	unburned
Permafrost	absent	present	present
Vegetation type	black spruce forest	burnt black spruce forest	mixed spruce and aspen
Depth of sensors (cm)	0, 50, 150	0, 50, 150, 200	0, 50, 100, 135
Core log	0–20 cm: organics	0–15 cm: burned organics	0–45 cm: organics, fibric to mesic
	20–110 cm: silt	15–200 cm: sandy silt	45–50 cm: ice
	110–150 cm: bedrock		50–100 cm: sandy silt w/ ice lenses up to 5 mm thick
			100–140 cm: silt grading to sand

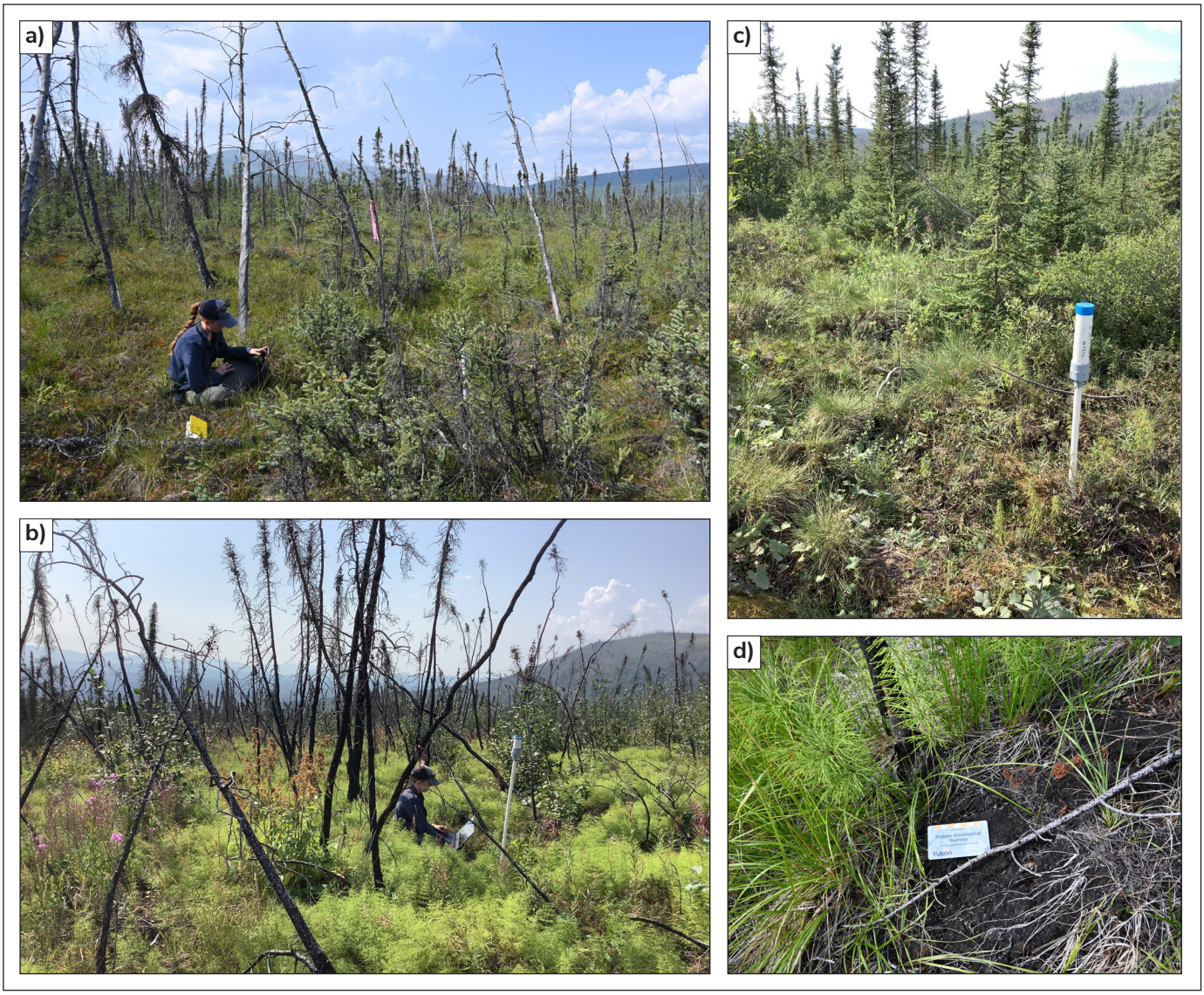

Figure 2. *Temperature monitoring stations in the study area:* **a)** *Ogilvie floodplain station,* **b)** *Eagle2 station (burned),* **c)** *Eagle1 station (unburned) and* **d)** *charred organic mat at Eagle2.*

content (W_d) was estimated using equation 2, based on Reynolds and Topp (2008),

$$W_d = \frac{m_i}{m_{ds}} \quad (2)$$

where m_i is the ice weight (measured as weight loss after drying) and m_{ds} is dry soil weight.

Aerial photos from unmanned aerial vehicle (UAV) surveys from each field visit along with 2020 lidar data (Government of Yukon, 2023) were used to track changes in landslide morphology over time. Agisoft Metashape was used to create structure-from-motion orthomosaics and digital elevation models (DEMs) of the landslides following a workflow designed by the United States Geological Survey (USGS; Over et al., 2021). The orthomosaics and DEMs were loaded into ArcGIS Pro and used to delineate retrogressive thaw flow headscarp movement from 2021 to 2023.

Timing of the landslides was investigated using air photos from the Government of Yukon air photo library dating from 1949 to 2007 (Yukon Energy, Mines and Resources, 2023) and PlanetLab satellite imagery from 2017 to 2023 (Planet Labs PBC, 2017–2023). The temporal resolution of satellite imagery varied between 1 and 3 days and was often cloud covered for multiple consecutive days. The initiation date for each landslide

was assigned using the first day that there was visible evidence of the landslide. It is important to note that nine new landslides were visible after a particularly long span of cloud-covered imagery between July 14 and 21, 2018. The exact initiation dates for these landslides were difficult to determine due to the cloudy imagery, so they were all assigned a July 22 initiation date. Landslide scars were delineated by polygons in ArcGIS Pro (Fig. 1) and points were used in initiation zones to calculate landslide characteristics.

Spectral differences between healthy vegetation and recently burned vegetation can be used to calculate a burn severity index. Healthy vegetation strongly reflects near-infrared light (NIR) and weakly reflects shortwave infrared (SWIR) light compared to burned vegetation. A normalized burn ratio (NBR; equation 3) was calculated using Landsat 8 imagery taken before and after the fire. The difference between the pre and post-fire NBR (differenced NBR, or dNBR) was used to calculate the burn severity of the fire (equation 4), which was then classified according to Key and Benson (2006), which is the USGS standard.

$$NBR = \frac{NIR - SWIR}{NIR + SWIR} \quad (3)$$

$$dNBR = \textit{pre-fire NBR} - \textit{post-fire NBR} \quad (4)$$

Results

Wildfire effects on permafrost depth and temperature

The study area experienced mostly low burn severity, with 30 to 100 m^2 patches of moderate to low-severity burn (Fig. 1). Ground temperature data from thermistors show that the depth to permafrost is approximately 100 cm in the Ogilvie floodplain (Fig. 3a). The burned site (Eagle2) reaches permafrost at a depth of 180 cm (Fig. 3b). The unburned borehole (Eagle1) does not reach permafrost, but it has a shallower depth than the other sites, extending only 150 cm below surface (Fig. 3c). Using second-order polynomial trendlines it can be inferred that the unburned Eagle1 site would reach permafrost at approximately 160 cm. The zone of zero amplitude is near 170 cm and the permafrost temperature is approximately –1°C. The inferred zone of zero amplitude for the burned site is much deeper, at approximately 210 cm; however, the permafrost temperature is also approximately –1°C. This indicates that although permafrost temperatures are likely to be similar between Eagle1 and Eagle2, Eagle1 reaches permafrost approximately 50 cm closer to surface than Eagle2 (burned). When comparing similar depths, the unburned and burned sites have similar average temperatures. The Ogilvie floodplain data has the shallowest depth to permafrost, and the zone of zero amplitude has a temperature of approximately –4°C. The measurements taken at 0 cm at all locations are likely inflated due to the influence of solar radiation on the sections of pipe that are above ground.

Active layer detachments

A total of 31 ALDs were identified in the study area between 1949 and 2013. This is likely an under-representation because the spatial and temporal resolution of the historical record is lower than that of more recent data. No obvious fire triggers were evident for these landslides, so they are interpreted to represent a background landslide rate. No landslides were identified between 2013 and 2016. The occurrence of 41 ALDs was identified during the period from the wildfire in 2017 and the end of 2018; one additional ALD was identified in 2020 (Fig. 4). This represents a fortyfold increase in landslides per year in the two years after the wildfire compared to the background landslide rate. Figure 5a and b show active layer detachment events relative to precipitation and temperature data from the Eagle Plains weather station. In 2017, the first ALD occurred 3 days after the wildfire and more than 50% of the total slides occurred during a two-week period in early August 2017, beginning just 20 days after the area was burned. During this two-week period, the weather station recorded increased precipitation (20% of the total summer rainfall) and average daily temperatures were 2°C higher than the average August temperature from 1980 to 2006.

In summer 2018, there were 16 ALDs. Almost all landslides occurred in July, with most initiating between July 13 and 25. The satellite imagery is cloud covered from July 14 to 21, coinciding with increased precipitation recorded at Eagle Plains. Landslides with the assigned date of July 22 may have occurred earlier during this eight-day cloudy period. Similar to 2017, these landslides became visible following high rainfall days. Daily average temperature reached its summer peak from July 22 to 25, coinciding with the initiation of

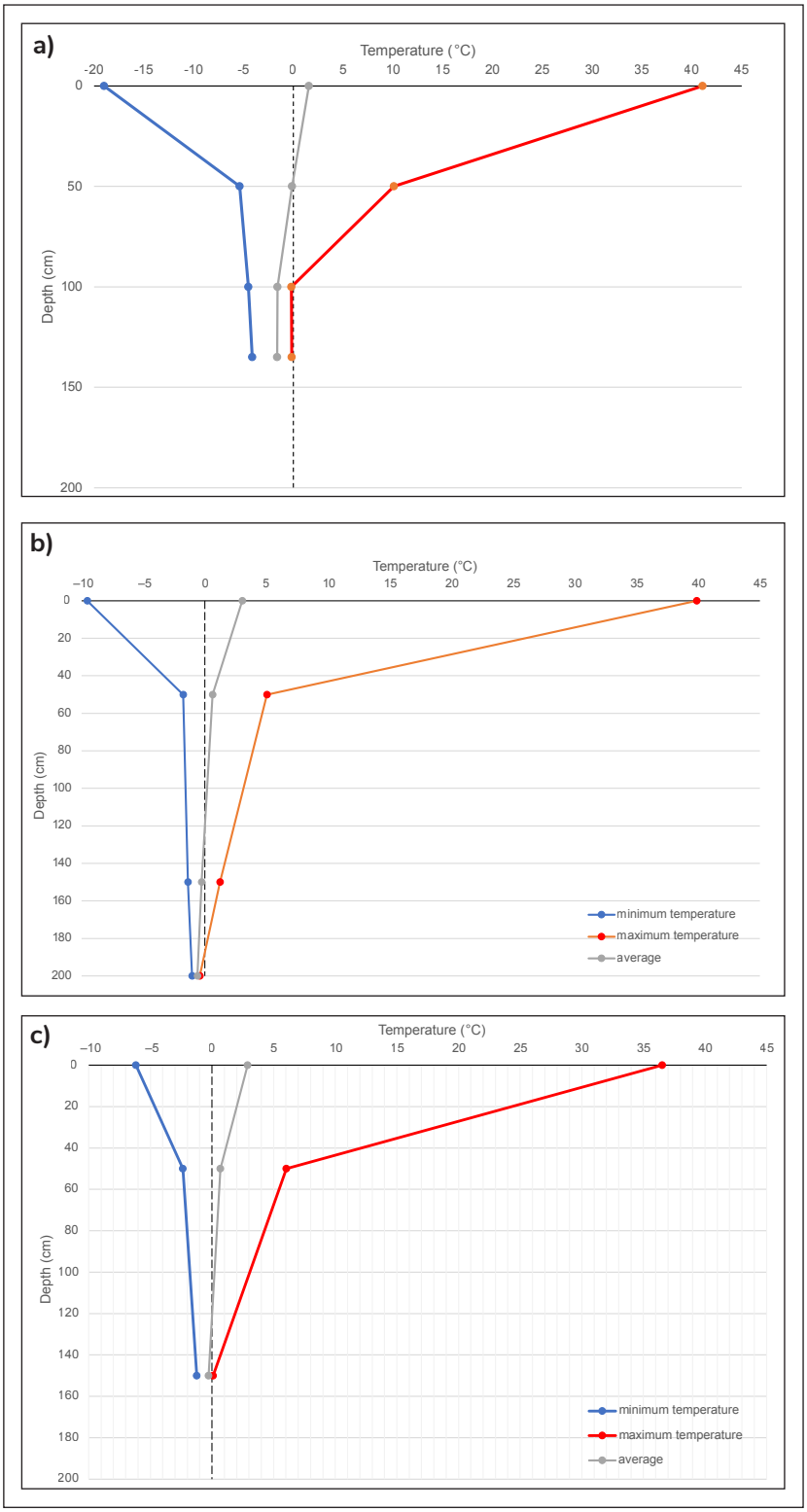

Figure 3. *Temperature envelopes plotted for* ***a)*** *Ogilvie floodplain,* ***b)*** *Eagle2 (burned) and* ***c)*** *Eagle1 (unburned) stations. Depth at which the red line crosses 0°C is the depth to permafrost. None of the borehole depths are deep enough to measure the permafrost temperature at the zone of zero amplitude where the minimum and maximum lines converge.*

three ALDs. From 2019 to 2023, only one ALD has been identified in the study area.

Active layer detachment characteristics are summarized in Table 2 and representative photos are shown in Figure 6. All ALDs within the study area occur on south and southwest-facing slopes. The landslide failure surfaces are relatively planar and parallel to topography; however, deep V-shaped, post-landslide incisions made by surface water erosion have modified this profile. The depths of the headscarps and initiation zones are relatively uniform, ranging from approximately 1 to 2 m. The runout distances of the ALDs range from 25 to 530 m, with the most extensive reaching the bottom of the slope. Two of the most extensive ALDs occurred in 2018, depositing debris on the highway and right of way that resulted in road closures (Fig. 6c). Those landslides that travelled to the bottom of the slope appear to have scoured deeper into the lower slope, entraining more material and forming levees of coarse debris on the sides of the landslide scars. Many of the ALDs experienced multiple stages of failure, with upslope retrogressions occurring in the days following the initial failure. Slope angles at the initiation point ranged from 9 to 45 degrees. Field investigations revealed that the initiation of ALDs commonly occurred in either shale-dominant colluvium or sandstone-dominant colluvium. Some headscarps exposed highly weathered shale bedrock at or below the failure plane. Bedrock exposed in the headscarps is classified as highly weathered according to the classification of rock weathering by Deere and Patton (1971), when more than half the rock material is decomposed and fresh rock is present as a discontinuous framework.

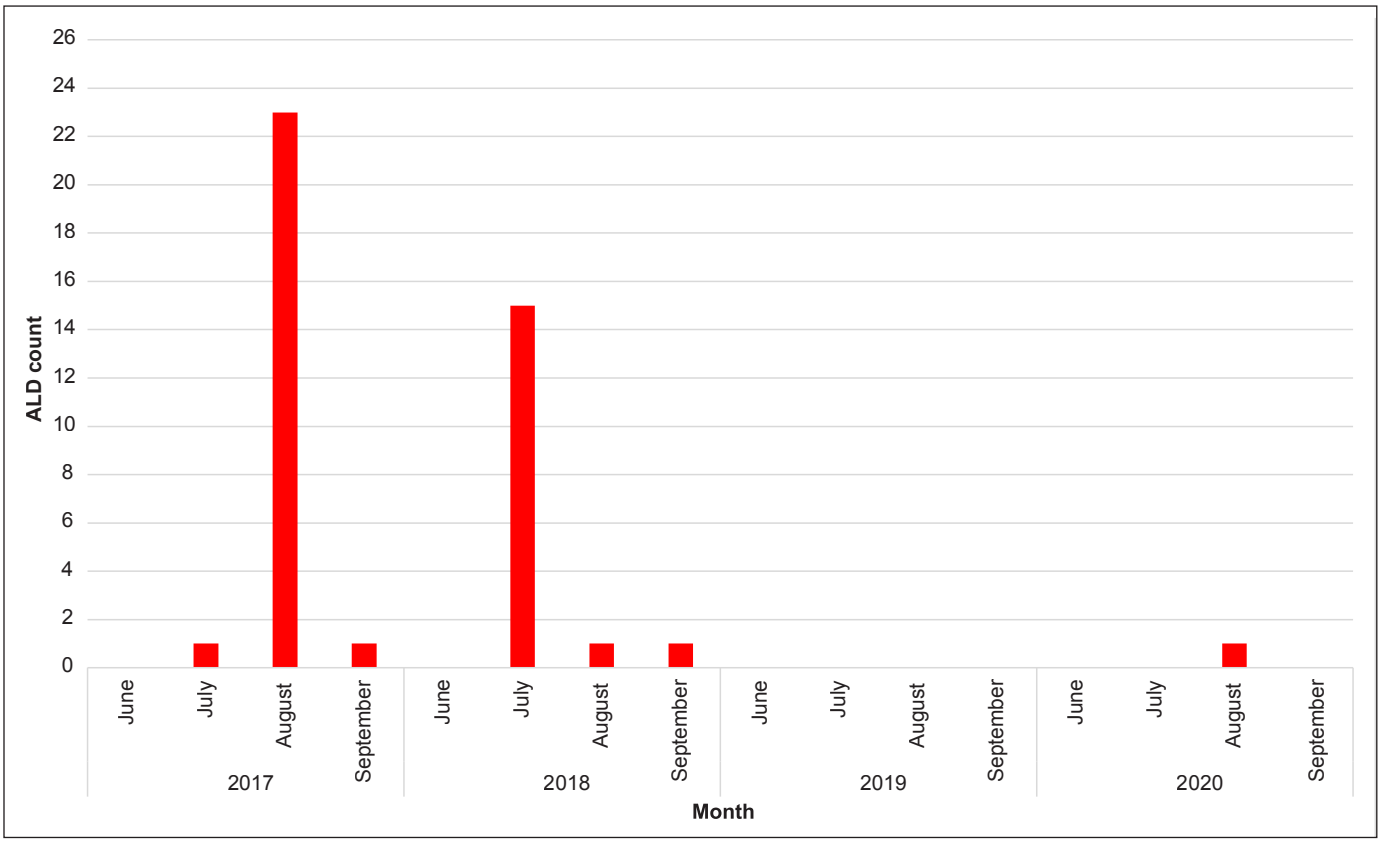

Figure 4. *Active layer detachment (ALD) events in the study area from 2017 to 2020. No ALDs were identified from 2021 to 2023.*

Retrogressive thaw flows

Six RTFs were identified in the study area; all were initiated after the 2017 wildfire. The exact initiation timing of the RTFs is difficult to constrain due to poor spatial resolution of available imagery and the slow nature of the slide progression. Retrogressive thaw flows appear to have started transporting sediment downslope during summer 2019 and all six are clear in lidar data obtained during summer 2020. Five of six RTFs are within close proximity in the west end of the study area; the sixth is near the east end of the study area (Fig. 7a). At the eastern end of the study area, RTF6 was the only landslide that did not appear to form in the path left by an ALD and had the lowest initiation slope angle (Fig. 7b). In 2023, the RTFs ranged in area from 1150 to 39 400 m^2. The average slope angle from the estimated initiation point is 14 degrees. Sediment transport and deposition from three RTFs reaches the bottom of the slope, causing blockages in backchannels and creeks that traverse the area between the slope and highway. This is shown in UAV imagery and was also observed on the ground as the waterways were found to have changed from the first field visit in early June to the last visit in late September (Fig. 7c). Four of the RTFs had massive ice bodies exposed in their headwalls. The two that did not have exposed ice were not as active throughout the 2023 site visits and exhibited patches of vegetation regrowth in the form of mosses and shrubs.

RTF1

In 2023, the largest and most active RTF in the study area was RTF1 (Fig. 7a). RTF1 was the only site selected for ice content sample collection because it has the most extensive exposures of stratigraphy and visibly ice-rich permafrost. This landslide has grown more than 200% in area (from headscarp to extent of deposition) and has retrogressed approximately 50 m/year between 2021 and 2023 (Fig. 8a). Detailed stratigraphy of RTF1 as well as the other RTFs is forthcoming in future work; however, the focus for this study is the variation in ice content between different surficial materials. The stratigraphy of the headwall and sidewalls of RTF1 is

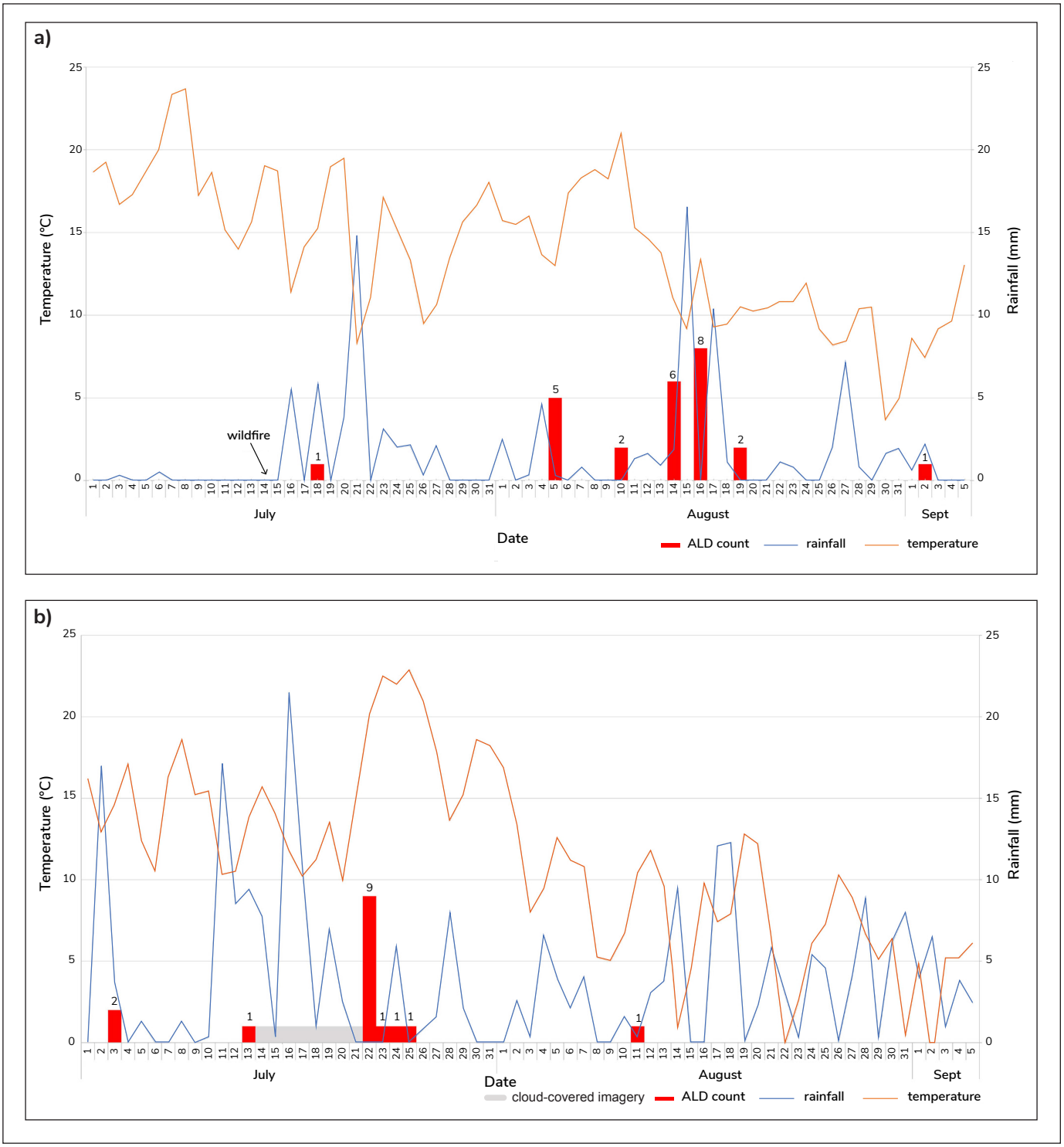

Figure 5. *Active layer detachment initiation dates for* ***a)*** *2017 and* ***b)*** *2018, plotted with temperature and rainfall data from the Eagle Plains weather station. Note: July 14 to 21, 2018, satellite imagery is cloud covered; active layer detachment events plotted on July 22 may have occurred up to eight days earlier.*

Table 2. *Characteristics of active layer detachment and retrogressive thaw flows.*

Landslide type		Landslide area (m^2)	Initiation elevation (masl)	Initiation slope (degrees)
Active layer detachment	mean	4389	622	27
	maximum	21 031.4	769	45
	minimum	318.3	519	9
	total	184 365		
Retrogressive thaw flow slide	mean	12 549	542	14
	maximum	39 401	521	24
	minimum	1150	562	4
	total	75 296		

complex and spatially variable (Fig. 8b, c). Colluvium and loess are the predominant materials; both range in clast content and amounts of organic matter. The colluvium units are up to 5 m thick and the loess packages range from 0.3 to 1.4 m. The headwalls also have extensive wedge ice, with exposures of up to 3 m vertical and 7 m horizontal in some sections. Most of the exposed headwall and sidewalls are frozen from 1 to 2 m below ground surface. Ice content of selected units is described in Table 3. The sample with the highest excess ice content is sample 2a from the lower part of a silty colluvium unit, with 65% volumetric excess-ice content and 121% gravimetric water content. Samples taken from unit 4 have the lowest ice content.

Discussion

Significance of bedrock

Initial observations indicate that there are important associations between ALDs and bedrock lithology in the study area. Because the region is unglaciated, bedrock is pervasively weathered on most slopes, resulting in thick blankets of bedrock-derived colluvium. The breakdown of the sedimentary rocks into finer materials such as silt and clay can decrease pore space, reducing water drainage through the slope. High ice content is more commonly associated with finer materials than with coarse materials (Jorgenson et *al*., 2008; French, 2017; O'Neill et *al*., 2019). Investigations of ALD initiation zones commonly revealed either sandstone-dominant colluvium or shale-dominant colluvium. In sandstone-dominant colluvium, ALDs initiate only on slopes greater than 30 degrees; whereas initiation angles ranged from 11 to 34 degrees in shale-dominant colluvium. The relatively high hydraulic conductivity of the sandstone compared to the low hydraulic conductivity of the shales may impact slope stability (Deere and Patton, 1971) and influence the permafrost conditions of the slope. Another factor to consider is the role of ice formation within weathered shale bedrock. Fine-grained sedimentary rocks allow segregated ice to form within fractures and bedding planes. This contributes to slope instability in two ways: ice formation within bedrock results in fracturing along the planes of weakness (Dyke, 1984); and increasing the ice content can lead to increased pore water pressure if the permafrost degrades (Eigenbrod et al., 1996).

Significance of topography in RTF formation

The national and global-scale model estimations for ground ice content are useful conceptual tools, but do not capture local-scale factors. As a result, initial observations from the field area indicate that ground ice content is significantly higher in some areas of the slope than the estimated 20% from the models (Heginbottom et al., 1995; O'Neill et al., 2022). The

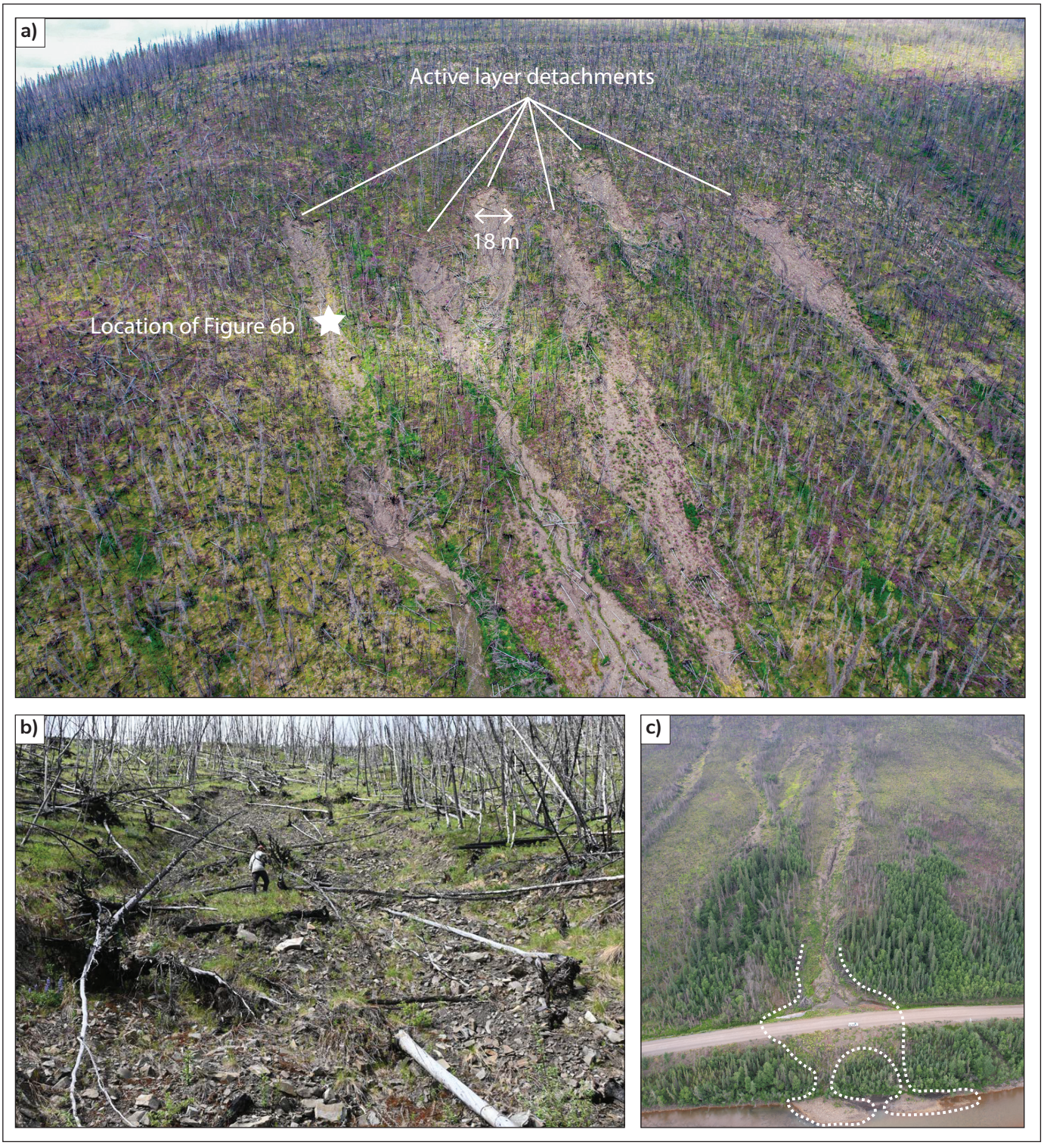

Figure 6. *Field images of active layer detachments (ALDs) in the study area:* **a)** *multiple parallel ALD scars initiating at approximately the same elevation, with varying run-out lengths. Photo taken in August 2023;* **b)** *upslope view of ALD indicated in a) with person for scale. Photo taken in June 2023;* **c)** *run out of one 2018 ALD, which crossed the Dempster Highway in 2018 and caused closures; white truck for scale, run out delineated by white dashed line. Photo taken in 2019.*

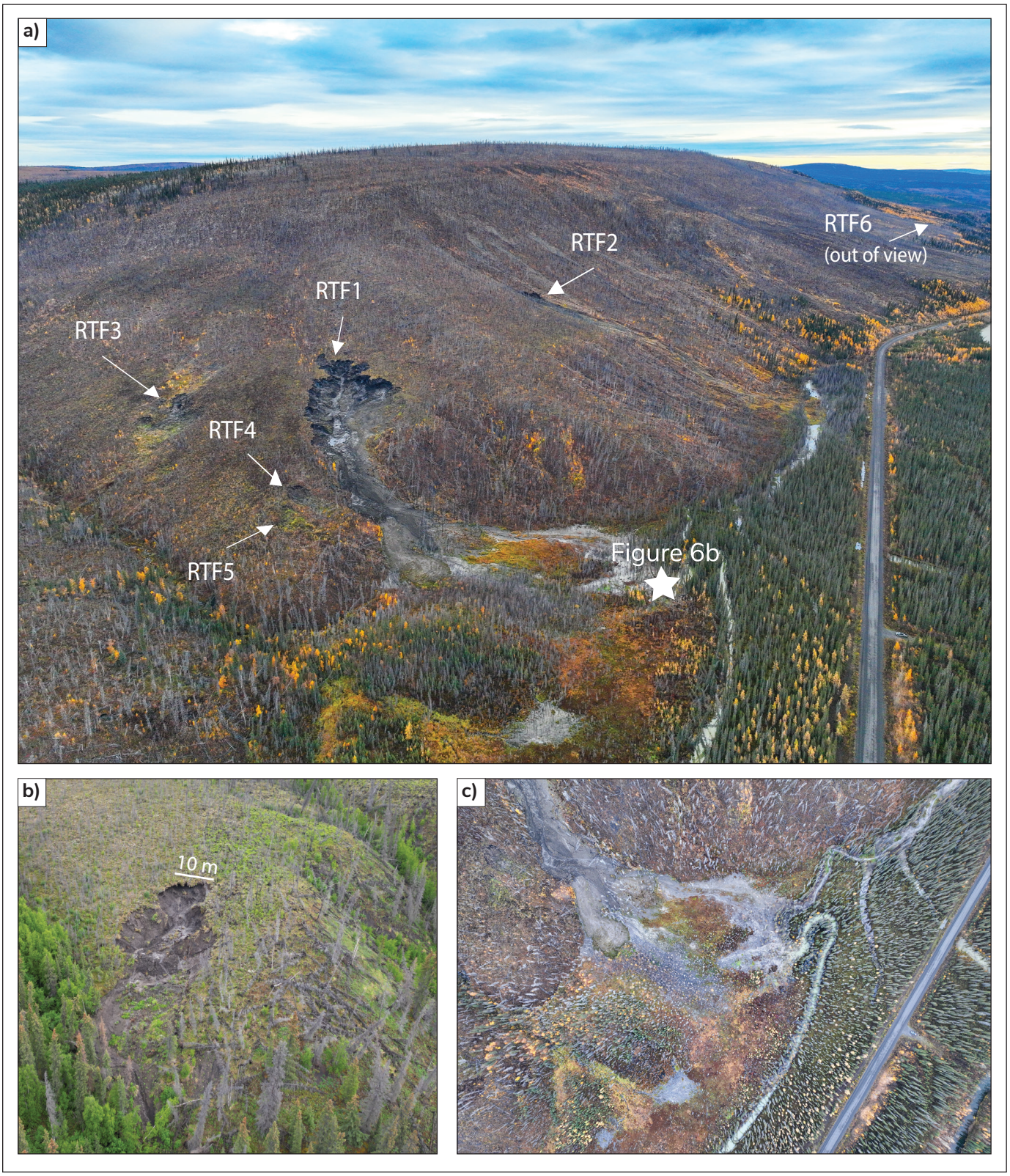

Figure 7. **a)** *View facing east of retrogressive thaw flow (RTF) locations in the study area in September 2023.* **b)** *View looking east showing RTF6, the only RTF in the east end of the study area. Photo taken June 2023.* **c)** *Sedimentation from RTF1 fills and blocks a creek at the base of the slope, resulting in flooding of the forest floor. Photo taken September 2023.*

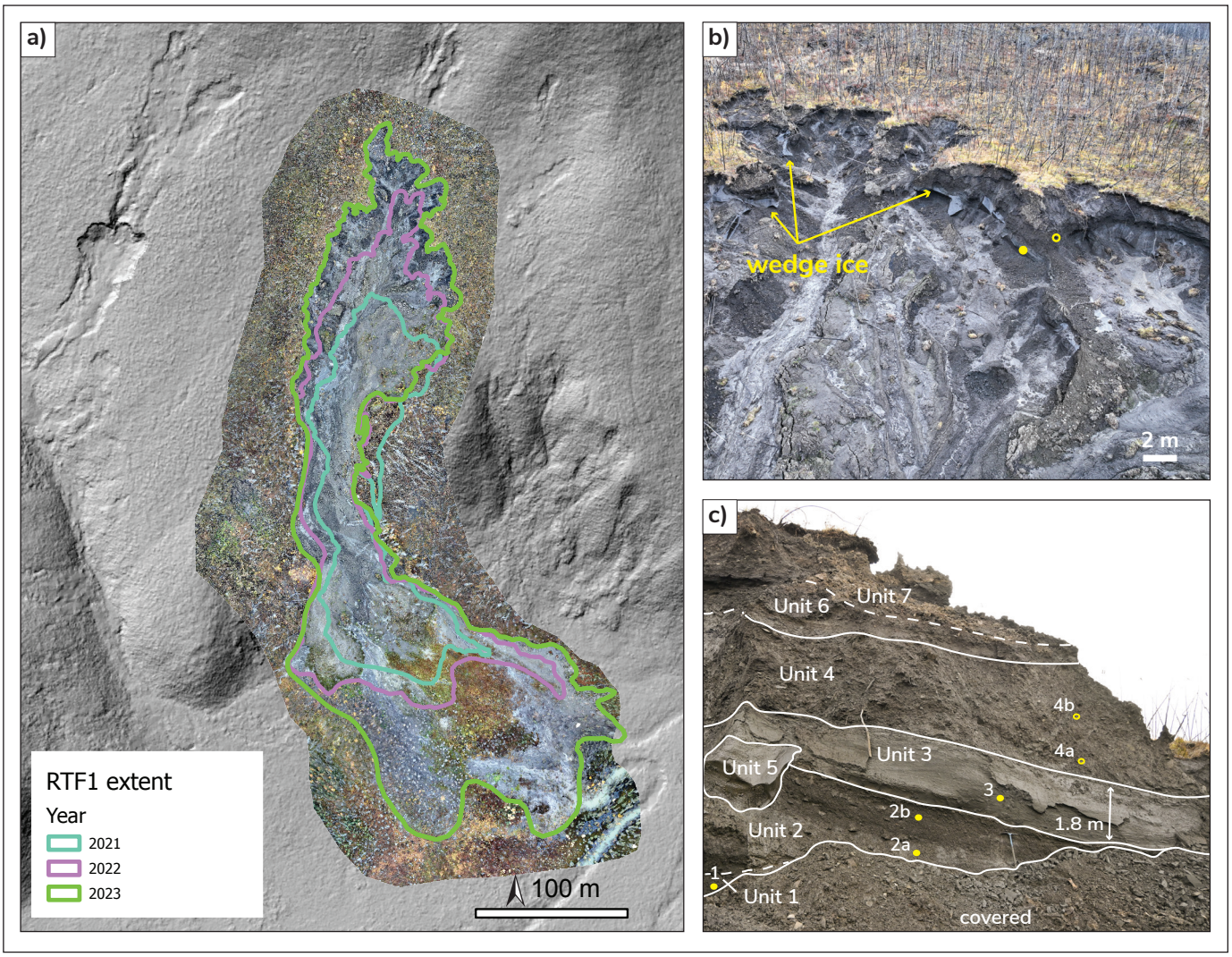

Figure 8. **a)** *Growth of RTF1 from 2021 to 2023 shown on 2023 orthomosaic overlying hillshade derived from lidar data (Government of Yukon, 2023).* **b)** *Oblique view of the RTF1 headscarp in September 2023 showing wedge ice and locations of ice content sampling. The solid yellow circle indicates the locations of samples 1 to 3 and the hollow yellow circle indicates the location of samples 4a and b.* **c)** *Close-up view of units sampled for ice content. Samples 4a and b (hollow yellow circles) were collected on the other side of the exposed rib. Photo taken September 2023.*

models generally account for the first 5 m below surface in their estimations and may not be able to account for multiple surficial materials within that depth. The headwalls and sidewalls of RTFs in the study area commonly expose ground ice, including metre-scale wedge ice at depths up to 8 m. The surficial material units also vary in composition and thickness within sites, each with varying ice contents. Retrogressive thaw flow formation in the study area is dependent on high ground-ice content to mobilize sediment and continue upslope retrogression; therefore, RTF formation appears to be a reasonable indicator for the presence of high ice content and fine-grained materials in certain areas of the slope. The RTFs formed on gently sloping terrain situated between steep upper and lower slopes. A possible reason for high ice content across this landform is the preferential accumulation of loess and colluvium, which supply ideal conditions for ice-wedge formation and preservation.

Wildfire, precipitation and temperature influences on landslide timing

The timing and frequency of the landslides in the study area are strong indicators that slope stability was impacted by the 2017 wildfire. Most of the ALDs

Table 3. *Ice content analysis of samples collected from RTF1, the largest and most active retrogressive thaw flow in the study area; sample locations are indicated in Figure 8b, c.*

Unit	Sample number	Unit thickness (cm)	Material	Frozen	Volumetric excess-ice content (%)	Gravimetric water content (%)
1	1	30 (lower contact covered)	silt	yes	39	64
2	2a	200	silty colluvium	yes	65	121
2	2b			yes	44	43
3	3	180	silt	yes	9	31
4	4a	470	organic-rich colluvium	yes	no supernatant water	20
4	4b			yes	3	8
5	n/a	variable: 10–300	wedge ice	yes	approximately 100	not measured
6	n/a	40	organic-rich silt	no	not sampled	not sampled
7	n/a	170	colluvium	no	not sampled	not sampled

occurred within weeks of the wildfire. During this period, the permafrost likely experienced rapid changes due to the direct heat from the fire and the increased absorption of incoming solar radiation caused by decreased shade, insulation and albedo. Active layer detachments in the summers of 2017 and 2018 may have also been influenced by precipitation and warm air temperatures. In 2018, peak annual rainfall was followed by peak summer temperatures, following which nine ALDs were identified. Air temperature and rainfall patterns in the summer of 2019 were similar to 2017 and 2018; however, even with distinct peaks in either temperature or precipitation, no new landslides were identified. This suggests that wildfire impacts had the strongest influence on slope stability in the study area relative to air temperatures and rainfall events. One small ALD took place in 2020 and shows no clear association with either precipitation or temperature. No RTFs were identified in the study area from 1949 to 2017; however, six RTFs initiated in the study area during the six years following the wildfire, and in 2023 all of them exhibited some degree of activity.

Hazard cascades

The study area is a unique example of the cascading effects of hazards in permafrost regions (Fig. 9). Here, a slope containing ice-rich permafrost experienced a wildfire, which decreased slope stability and resulted in numerous ALDs. The resultant exposure of permafrost triggered the initiation of RTFs in subsequent years, all of which are still active today. The RTFs have deposited large amounts of sediment and caused an influx of water at the base of the slope, altering drainage patterns and flooding the forest next to the highway. The impacts of increased water in the area are yet to be fully realized; however, it could lead to further degradation of permafrost and subsidence in the valley bottom near the road.

Degradation of permafrost is a negative cycle of its own in which carbon and methane previously stored in frozen ground are released into the atmosphere, where they contribute to the amplification of climate change. The impacts of permafrost-related landslides in the study area go beyond the burn area and the

Figure 9. *Cascading impacts of wildfire in permafrost terrain in the study area. Wildfire leads to active layer detachments (black arrows), which expose ice-rich permafrost, resulting in retrogressive thaw flow (white hatched lines show headscarps) that deposit large volumes of sediment and water at the base of the slope (white dotted outlines), and further degrade permafrost in the valley bottom. Photo taken in 2023.*

visible outline of the landslide scars. These processes and feedback loops highlight the fragility of northern communities and infrastructure in a changing climate.

Conclusions

This study investigated permafrost-related landslides following a 2017 wildfire on a slope along the Dempster Highway in the Yukon. A 39% increase in ALDs was observed within the two years following the fire, suggesting the burn significantly influenced slope stability. Increased precipitation and air temperatures appear to have contributed to slope instability in both 2017 and 2018. No RTFs were identified between 1949 and 2016, although the spatial and temporal resolution of the historical data may not be sufficient to detect these types of landslides. Six RTFs were identified after the wildfire in areas that were burned and/or disturbed by ALDs. Retrogressive thaw flow development is not discernible until summer 2019. The largest RTF retrogressed 100 m between 2021 and 2023. The ALDs and RTFs in the study area have brought debris onto the highway and increased sediment and water volume at the base of the slope, potentially causing further permafrost degradation. Results from this study indicate that wildfire on permafrost slopes can initiate a

cascading hazard effect that can be further influenced by local precipitation and warm summer temperatures. Further research is needed to quantify the predictive relationship between bedrock lithology, surficial material and permafrost characteristics with respect to landslide initiation.

Acknowledgments

This study took place in the Traditional Territories of the Vuntut Gwitchin and the Tr'ondëk Hwëch'in First Nations. The authors would like to thank members of the Tr'ondëk Hwëch'in First Nation, as well as Royce Freeman at Highways and Public Works, Government of Yukon, for helpful and insightful discussions. Thank you to the staff at the Ogilvie maintenance camp on the Dempster Highway for providing food and lodging during fieldwork. We thank Moya Painter of YGS for providing field assistance and Brendan Murphy for assisting in burn severity assessments. This project is supported by the Yukon Geological Survey and Polar Canada's Northern Scientific Training Program. A detailed review by Kristen Kennedy considerably improved the manuscript.

References

Burn, C.R., 1994. Permafrost, tectonics, and past and future regional climate change, Yukon and adjacent Northwest Territories. Canadian Journal of Earth Sciences, vol. 31, no. 1, p. 182–191. https://doi.org/10.1139/e94-015

Burn, C.R. and Lewkowicz, A.G., 1990. Canadian landform examples – 17: Retrogressive thaw slumps. Canadian Geographic, vol. 34, p. 967–981.

Burn, C.R., Moore, J., O'Neill, H.B., Hayley, D., Trimble, J., Calmels, F., Orban, S.N., Idrees, M., 2015. Permafrost characterization of the Dempster Highway, Yukon and Northwest Territories. *In:* Proceedings, 68th Canadian Geotechnical Conference and 7th Canadian Permafrost Conference, Paper 703, 21-23 September 2015, Quebec City, QC, Canadian Geotechnical Society, Richmond, BC, 8 p.

Calmels, F., Roy, L.P., Laurent, C., Amyot, F., Cubley, J. and Lipovsky, P., 2021. Assessment and Monitoring of a New Retrogressive Thaw Slump at km 1456 of the Alaska Highway: A Rare Opportunity. YukonU Research Centre, Yukon University, Whitehorse, 72 p. https://www.yukonu.ca/sites/default/files/inline-files/PGR_2021_01_Tak_Slump_NTAI_0.pdf

Climate Atlas of Canada, 2019. Climate Change in Canada, version 2. Prairie Climate Centre, University of Winnipeg, Winnipeg, Manitoba, https://climateatlas.ca [accessed November 25, 2023].

Coates, J., 2008. The impact of forest fire on permafrost slopes Klondike area, Yukon Territory. MSc thesis, University of Ottawa, Ontario, Canada, 218 p. https://doi.org/10.20381/ruor-18782

Deere, D. and Patton, F., 1971. Slope stability in residual soils. *In*: Proceedings of the 4th Panamerican Conference on Soil Mechanics and Foundation Engineering, vol. 1: State-of-the-Art Papers. American Society of Civil Engineers, New York, p. 87–170.

Dixon, J., 1992. Stratigraphy of Mesozoic strata, Eagle Plain area, northern Yukon. Geological Survey of Canada, Bulletin 408, 58 p. https://doi.org/10.4095/133639

Duk-Rodkin, A. and Hughes, O.L., 1995. Quaternary geology of the northeastern part of the central Mackenzie Valley Corridor, District of Mackenzie, Northwest Territories. Geological Survey of Canada Bulletin 458, 45 p.

Dyke, L., 1984. Frost heaving of bedrock in permafrost regions. Environmental and Engineering Geosciences, vol. 21, no. 4, p. 389–405. https://doi.org/10.2113/gseegeosci.xxi.4.389

Eigenbrod, K.D., Knutsson, S. and Sheng, D., 1996. Pore-water pressures in freezing and thawing fine-grained soils. Journal of Cold Regions Engineering, vol. 10, no. 2, p. 77–92. https://doi.org/10.1061/(ASCE)0887-381X(1996)10:2(77)

Environment Canada, 2023. Environment and Climate Change Canada Historical Climate Data. https://climate.weather.gc.ca/ [accessed November 10, 2023]

French, H.M., 1974. Active thermokarst processes, eastern Banks Island, western Canadian Arctic. Canadian Journal of Earth Sciences, vol. 11, no. 6, p. 785–794. https://doi.org/10.1139/e74-078

French, H.M., 2017. The Periglacial Environment, Fourth Edition. Wiley-Blackwell, New Jersey, 544 p.

Government of Yukon, 2023. Lidar collection. https://maps.mcelhanney.com/Vertisee/YukonGovLidar/ [accessed January 2023].

Guthrie, R.D., 2001. Origin and causes of the mammoth steppe: A story of cloud cover, woolly mammal tooth pits, buckles, and inside-out Beringia. Quaternary Science Reviews, vol. 20, p. 549–574. https://doi.org/10.1016/S0277-3791(00)00099-8

Hanes, C.C., Wang, X., Jain, P., Parisien, M.-A., Little, J.M. and Flannigan, M.D., 2019. Fire-regime changes in Canada over the last half century. Canadian Journal of Forest Research, vol. 49, no. 3, p. 256–269. https://doi.org/10.1139/cjfr-2018-0293

Heginbottom, J.A., Dubreuil, M.A. and Harker, P.A., 1995. Canada, Permafrost. *In*: The National Atlas of Canada (5th edition), Natural Resources Canada, Geomatics Canada, MCR Series no. 4177, 1 sheet. https://doi.org/10.4095/294672

Holloway, J., Lewkowicz, A., Douglas, T., Li, X., Turetsky, M., Baltzer, J. and Jin, H., 2020. Impact of wildfire on permafrost landscapes: A review of recent advances and future prospects. Permafrost and Periglacial Processes, vol. 31, no. 3, p. 371–382. https://doi.org/10.1002/ppp.2048

Jones, M.K.W., Pollard, W.H. and Giguère, N., 2021. Daily Field Observations of Retrogressive Thaw Slump Dynamics in the Canadian High Arctic. Arctic, vol. 74, p. 339–354.

Jorgenson, M.T., Romanovsky, V., Harden, J., Shur, Y., O'Donnell, J., Schuur, E.A.G., Kanevskiy, M. and Marchenko, S., 2010. Resilience and vulnerability of permafrost to climate change. Canadian Journal of Forest Research, vol. 40, no. 7, p. 1219–1236. https://doi.org/10.1139/X10-060

Jorgenson, T., Yoshikawa, K., Kanevskiy, M., Shur, Y., Romanovsky, V., Marchenko, S., Grosse, G., Brown, J. and Jones, B., 2008. Permafrost Characteristics of Alaska. *In:* The Ninth International Conference on Permafrost, Fairbanks, Alaska, p. 121–122.

Kennedy, K.E., Froese, D.G., Zazula, G.D. and Lauriol, B., 2010. Last Glacial Maximum age for the northwest Laurentide maximum from the Eagle River spillway and delta complex, northern Yukon. Quaternary Science Reviews, vol. 29, no. 9–10, p. 1288–1300. https://doi.org/10.1016/j.quascirev.2010.02.015

Key, C. and Benson, N., 2006. Landscape Assessment (LA). *In*: D.C. Lutes, R.E. Keane, J.F. Caratti, C.H. Key, N.C. Benson, S. Sutherland and L.J. Gangi. FIREMON: Fire effects monitoring and inventory system. Gen. Tech. Rep. RMRS-GTR-164-CD. Fort Collins, CO: U.S. Department of Agriculture, Forest Service, Rocky Mountain Research Station, p. LA-1-55

Kokelj, S.V. and Burn, C.R., 2003. Ground ice and soluble cations in near-surface permafrost, Inuvik, Northwest Territories, Canada. Permafrost and Periglacial Processes, vol. 14, no. 3, p. 275–289. https://doi.org/10.1002/ppp.458

Kokelj, S.V., Tunnicliffe, J., Lacelle, D., Lantz, T.C. and Fraser, R.H., 2015. Retrogressive thaw slumps: From slope process to the landscape sensitivity of northwestern Canada. *In:* Proceedings, 68th Canadian Geotechnical Conference and 7th Canadian Permafrost Conference, Paper 104, 21–23 September 2015, Quebec City, QC, Canadian Geotechnical Society, Richmond, BC, 8 p.

Lacelle, D., Brooker, A., Fraser, R.H. and Kokelj, S.V., 2015. Distribution and growth of thaw slumps in the Richardson Mountains–Peel Plateau region, northwestern Canada. Geomorphology, vol. 235, p. 40–51. https://doi.org/10.1016/j.geomorph.2015.01.024

Lantuit, H. and Pollard, W., 2007. Fifty years of coastal erosion and retrogressive thaw slump activity on Herschel Island, Southern Beaufort Sea, Yukon Territory, Canada. Geomorphology, vol. 95, p. 84–102. https://doi.org/10.1016/j.geomorph.2006.07.040

Lewkowicz, A., 1990. Morphology, frequency and magnitude of active layer detachment slides, Fosheim Peninsula, Ellesmere Island, N.W.T. Nordicana, vol. 54, p. 111–118.

Lewkowicz, A.G. and Harris, C., 2005a. Morphology and geotechnique of active-layer detachment failures in discontinuous and continuous permafrost, northern Canada. Geomorphology, vol. 69, p. 275–297. https://doi.org/10.1016/j.geomorph.2005.01.011

Lewkowicz, A.G. and Harris, C., 2005b. Frequency and magnitude of active-layer detachment failures in discontinuous and continuous permafrost, northern Canada. Permafrost and Periglacial Processes, vol. 16, p. 115–130. https://doi.org/10.1002/ppp.522

Lipovsky, P.S., Coates, J., Lewkowicz, A.G., Trochim, E., 2005. Active-layer detachments following the summer 2004 forest fires near Dawson City, Yukon. *In:* Yukon Exploration and Geology 2005, D.S. Emond, G.D. Bradshaw, L.L. Lewis and L.H. Weston (eds.), Yukon Geological Survey, p. 175-194.

O'Neill, H.B., Wolfe, S.A. and Duchesne, C., 2019. New ground ice maps for Canada using a paleogeographic modelling approach. The Cryosphere, vol. 13, no. 3, p. 753–773. https://doi.org/10.5194/tc-13-753-2019

O'Neill, H.B., Wolfe, S.A. and Duchesne, C., 2022. Ground ice map of Canada version 1.1. Geological Survey of Canada, Open File 8713, p. 7 (1 sheet). https://doi.org/10.4095/330294

Over, J.-S.R., Ritchie, A.C., Kranenburg, C.J., Brown, J.A., Buscombe, D.D., Noble, T., Sherwood, C.R., Warrick, J.A. and Wernette, P.A., 2021. Processing coastal imagery with Agisoft Metashape Professional Edition, version 1.6—Structure from motion workflow documentation. United States Geological Survey, Open-File Report 2021-1039, 46 p. https://doi.org/10.3133/ofr20211039

Perrin, A. and Jolkowski, D., 2022. Yukon Climate Change Indicators and Key Findings 2022. YukonU Research Centre, Yukon University, Whitehorse, 126 p.

Planet Labs PBC, 2017–2023. Planet Application Program Interface: In Space for Life on Earth. https://www.planet.com/ [accessed July 2023].

Reynolds, W.D. and Topp, G.C., 2008. Soil water analyses: principles and parameters. *In*: Soil Sampling and Methods of Analysis, 2nd ed., M.R. Carter and E.G. Gregorich (eds.), Canadian Society of Soil Science, Pinawa, MB, Canada, p. 913-937.

Schuur, E., McGuire, A.D., Schädel, C., Grosse, G., Harden, J., Hayes, D.J., Hugelius, G., Koven, C., Kuhry, P., Lawrence, D., Natali, S., Olefeldt, D., Romanovsky, V., Schaefer, K., Turetsky, M., Treat, C. and Vonk, J., 2015. Climate change and the permafrost carbon feedback. Nature, vol. 2015, p. 171–179. https://doi.org/10.1038/nature14338

Smith, C.A.S., Meikle, J.C. and Roots, C.F. (eds), 2004. Ecoregions of the Yukon Territory: Biophysical properties of Yukon landscapes. Agriculture and Agri-Food Canada, PARC Technical Bulletin no. 04-01, Summerland, British Columbia, 313 p.

Smith, S.L., O'Neill, H.B., Isaksen, K., Noetzli, J. and Romanovsky, V.E., 2022. The changing thermal state of permafrost. Nature Reviews Earth and Environment, vol. 3, p. 10–23. https://doi.org/10.1038/s43017-021-00240-1

Vincent, W.F., 2020. Arctic climate change: Local impacts, global consequences, and policy implications. *In*: The Palgrave Handbook of Arctic Policy and Politics, K.S. Coates and C. Holroyd (eds.), Springer International Publishing, Palgrave Macmillan, Cham, p. 507–526. https://doi.org/10.1007/978-3-030-20557-7_31

Wotton, B.M., Flannigan, M.D. and Marshall, G.A., 2017. Potential climate change impacts on fire intensity and key wildfire suppression thresholds in Canada. Environmental Research Letters, vol. 12, no. 9, 12 p. https://doi.org/10.1088/1748-9326/aa7e6e

Yukon Energy, Mines and Resources, 2023. Air photo library. Yukon Energy, Mines and Resources. https://yukon.ca/en/science-and-natural-resources/research-and-monitoring/find-air-photos-yukon [accessed July 2023].

Yukon Wildland Fire Report, 2017. Map compiled by Wildland Fire Management, Department of Community Services, Government of Yukon, 3 p. https://yukon.ca/en/2017-yukon-wildfire-map [accessed October 2023].